University of Glasgow

DEPARTMENT OF

AEROSPACE ENGINEERING

Inverse Simulation
Incorporating the Conceptual Simulation Model

Stephen Rutherford, Dr. Douglas G. Thomson

Internal Report No. 9428

December 1994

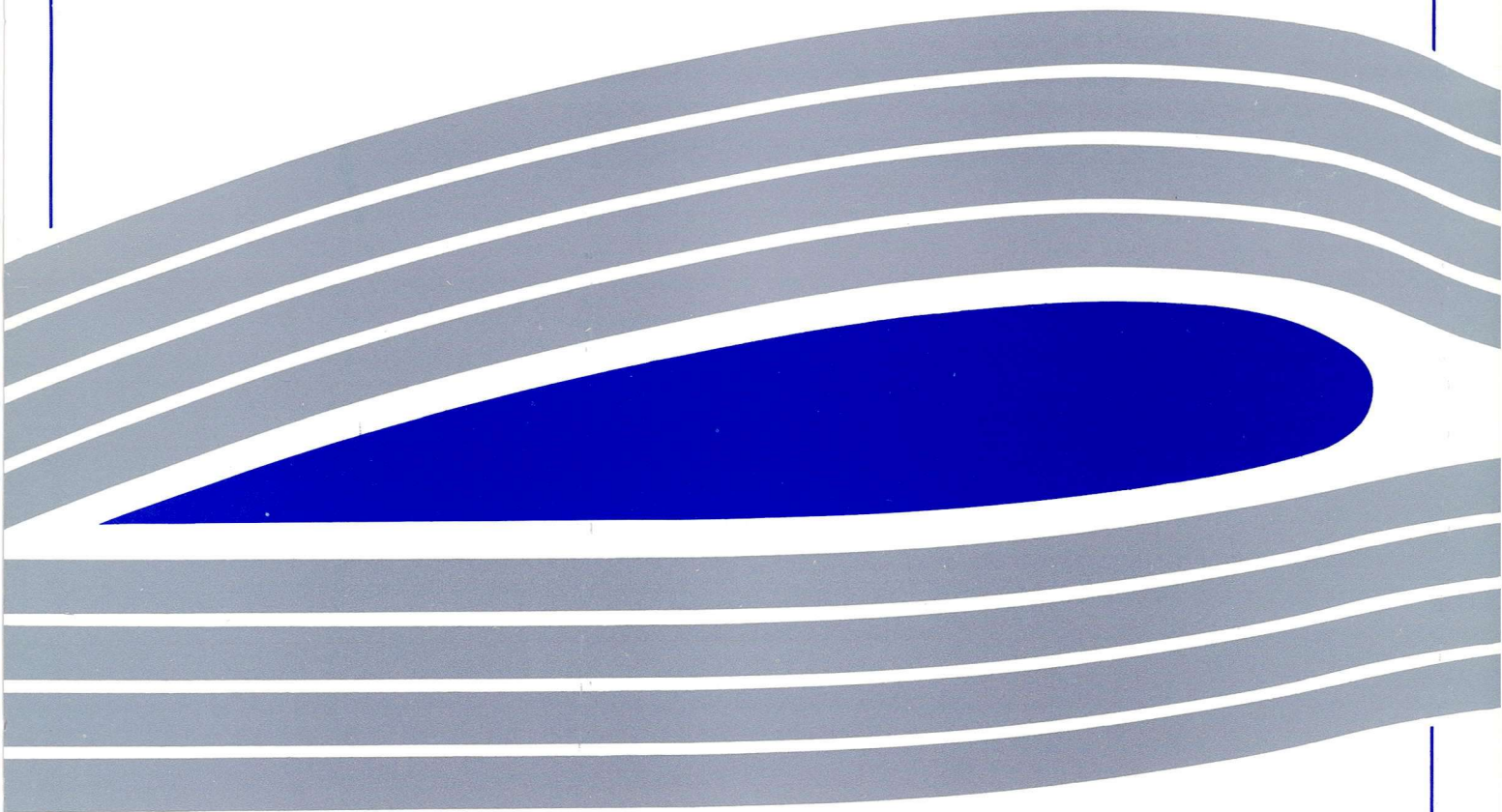

Inverse Simulation
Incorporating the Conceptual Simulation Model

Stephen Rutherford, Dr. Douglas G. Thomson

Internal Report No. 9428
December 1994

Summary

This report documents the application of the inverse simulation algorithm *Genisa* [1] to the Conceptual Simulation Model developed at DRA Bedford. The CSM is a simple, decoupled helicopter model used to investigate advanced control systems. As the aim was primarily to test the practicalities of the CSM in inverse simulation, no attempt has been made here to qualify the model, which is described in Appendix A and more fully in reference [2]. The Lateral Jinking manoeuvre is used to generate all results. Helicopter configurational data is similar to a Westland Lynx.

Contents

page no.

Nomenclature

a_0	rotor lift-curve slope	(1/rad)
C_T	rotor thrust coefficient	
$C_{T\ inflow}$	simplified thrust coeff. used for inflow calculation	
C_X	rotor X force coeff.	
C_{XF}, C_{YF}	fuselage X and Y force coeffs.	
g	acceleration due to gravity	(m/s^2)
G_p, G_{p^3}	roll rate demand linear and cubic gains	(rad/s)
G_q, G_{q^3}	pitch rate demand linear and cubic gains	(rad/s)
G_r, G_{r^3}	yaw rate demand linear and cubic gains	(rad/s)
G_η, G_ξ, G_ζ	pitch, roll and yaw inceptor gains	
l_1, ..., n_3	direction cosines for Euler transformation	
m	helicopter mass	(kg)
m_{TC}, n_{TC}	pitch and yaw acceleration input for turn coordination	(m/s^2)
p, q, r	components of helicopter angular velocity at centre of gravity	(rad/s)
p_{DEM} ... r_{DEM}	roll, pitch and yaw demand	(rad/s)
R	rotor radius	(m)
s	rotor solidity	
S_{XF}, S_{YF}	fuselage frontal and side area	(m^2)
t_1, t_2, t_3	time taken to complete sections of lateral jinking manoeuvre	(s)
u_B, v_B, w_B	reference body axes velocity components	(m/s)
u_{BR}, w_{BR}	velocity components resolved into rotor disc axes	(m/s)
V_F	resultant airspeed at fuselage in presence of rotor downwash	(m/s)
V_T	true airspeed	(m/s)
w_I	induced upwash	(m/s)
x_E, y_E, z_E	displacements relative to the earth fixed inertial frame	(m)
X, Y, Z	X, Y, Z forces	(N)
$\Delta Z_{ROT_{TC}}$	incremental rotor thrust for turn coordination	(N)

Greek Symbols

α	angle of attack	(rad)
α_F	fuselage incidence in presence of rotor downwash	(rad)
β	sideslip	(rad)
γ	flight path angle	(rad)
δ_C	collective pitch input	
$\delta_{C_{TC}}$	incremental collective pitch for turn coordination	

δ_0	rotor drag factor	
δ_2	rotor thrust dependent drag factor	
η, ξ, ζ	pitch, roll and yaw control inputs	
ϕ, θ, ψ	body roll, pitch and sideslip attitude angles	(rad)
θ_{SHAFT}	rotor shaft tilt angle	(rad)
ϕ_{TC}, ϕ_{MAX}	bound and maximum bank angle	(rad)
λ_0	normalised induced downwash	
μ, μ_z	in plane and normal to plane normalised velocities	
ρ	air density	(kg/m^3)
τ_a	actuator time constant	(s)
Ω	angular velocity of main rotor	(rad/s)

Vectors and Matrices

x	state vector
y	output vector
u	input vector
[J]	Jacobian matrix

Subscripts and Prefices

CALC, DES	calculated and desired values
ERR	error term
FUS, ROT	fuselage, rotor
TC	turn coordination
e	equilibrium or trim component
i, j	matrix indices
k	solution point
m	iteration number

1. *Genisa* : Generic Inverse Simulation Algorithm

1.1 Introduction

Inverse simulation can be used to predict a set of control inputs that will cause a predefined displacement of a subject vehicle. More specifically, in mathematically defining some desired vehicle manoeuvre or flight path the algorithm will solve the equations of motion for a unique time history of control inputs. This contrasts with *conventional simulation*, which calculates the vehicle state variables (and consequently flight path) in response to imposed control inputs. A formal definition can be obtained by considering the initial value problem which expresses the relationship between state, control and output vectors of a dynamic system and forms the basis of most vehicle simulations :

$$\dot{\mathbf{x}} = \mathbf{f}(\mathbf{x}, \mathbf{u}); \quad \mathbf{x}(0) = \mathbf{x_e} \tag{1}$$

$$\mathbf{y} = \mathbf{g}(\mathbf{x}). \tag{2}$$

The equations of motion (1) permit prediction of the behaviour of the state vector $\mathbf{x}$ in response to an imposed control vector $\mathbf{u}$ over a specified time period, $\mathbf{x_e}$ containing the state variables at t = 0. The output equation (2) states how the output vector $\mathbf{y}$ can be obtained from the state vector. Specific representations of equations (1) and (2), relating to the CSM, can be found in §2. These equations also summarise inverse simulation, which predicts the control vector $\mathbf{u}$ that will produce a desired output vector $\mathbf{y}$, and in doing so, the corresponding state vector $\mathbf{x}$.

1.2 Generic Inverse Simulation Algorithm

In *Genisa* the initial solution occurs at t = 0. The value of $\mathbf{x_e}$ is calculated for a specified trim condition and the first estimate of $\mathbf{u}$ taken as the trim value $\mathbf{u_e}$. In the general case (the m^{th} estimate at the k^{th} time point) $\dot{\mathbf{x}}(t_k)_m$ can be evaluated using $\mathbf{x}(t_k)$ and the current estimate for $\mathbf{u}(t_k)_m$

$$\dot{\mathbf{x}}(t_k)_m = \mathbf{f}[\mathbf{x}(t_k), \mathbf{u}(t_k)_m]. \tag{3}$$

This in turn can be integrated, using a Runge-Kutta method for example, to produce estimates of $\mathbf{x}(t_{k+1})_m$ and $\mathbf{y}(t_{k+1})_m$ at the next time point.

$$\mathbf{x}(t_{k+1})_m = \int_{t_k}^{t_{k+1}} \dot{\mathbf{x}}[(t_k)_m]\, dt + \mathbf{x}(t_k)_m \tag{4}$$

$$\mathbf{y}(t_{k+1})_m = \mathbf{g}\,[\mathbf{x}(t_{k+1})_m] \tag{5}$$

As the basis for a Newton-Raphson solution, an error function is defined as the difference between the latest estimate of the output vector, $\mathbf{y}(t_{k+1})_m$ and the desired value, $\mathbf{y_{DES}}(t_{k+1})$, that represents the prescribed flight path

$$\mathbf{y_{ERR}}(t_{k+1})_m = \mathbf{y}(t_{k+1})_m - \mathbf{y_{DES}}(t_{k+1}). \tag{6}$$

The function is tested against a predefined tolerance. If less then the tolerance then the programme moves on the next solution point k+1 and continues from equation (3). However if $\mathbf{y_{ERR}}(t_{k+1})_m$ is greater than the tolerance then a Jacobian is calculated and using its inverse, a new estimate of the control vector $\mathbf{u}(t_k)_{m+1}$ can be found (7). The Jacobian is a matrix evaluated by differentiating the output vector with respect to the control vector (8).

$$\mathbf{u}(t_k)_{m+1} = \mathbf{u}(t_k)_m - [\mathbf{J}]^{-1}\, \mathbf{y_{ERR}}(t_{k+1})_m \tag{7}$$

$$[\mathbf{J}] = \frac{d\, \mathbf{y}(t_{k+1})_m}{d\, \mathbf{u}(t_k)_m} \tag{8}$$

This new estimate is then used to calculate $\dot{\mathbf{x}}(t_k)_{m+1}$ and consequently the error function $\mathbf{y_{ERR}}(t_{k+1})_{m+1}$ within the m loop, m = m + 1. The programme is finished at the end of the manoeuvre time period (k=n).

1.3 Alternative Optimal Solution

The method described in §1.2 is valid only for situations where the number of known states (i.e. the manoeuvre constraints) is equal to the number of unknown controls. In such circumstances the Jacobian, **[J]** is square and readily inverted. There are alternative situations, however, where the Jacobian is rectangular and an exact solution of equation (6) does not exist, though as will now be described it is possible to rearrange the algorithm into a form for which an optimal solution can be found. From equation (8) it can be seen that,

$$[\mathbf{J}]\, \mathbf{u}(t_k)_m = \mathbf{y}(t_{k+1})_m \tag{9}$$

which is linear. Clearly from (9) the desired solution is a value of $\mathbf{u}(t_k)_m$, $\mathbf{u_{DES}}(t_k)$, which will produce $\mathbf{y}(t_{k+1})_m$ equal to $\mathbf{y_{DES}}(t_{k+1})_m$ i.e. solution of the following equation :

$$[\mathbf{J}]\,\mathbf{u}(t_k)_m - \mathbf{y_{DES}}(t_{k+1})_m = \mathbf{y_{ERR}}(t_{k+1})_m. \tag{10}$$

Equation (10) can be put in a more convenient form. In the region local to the solution, equation (8) can also be expressed as,

$$[\mathbf{J}] = \frac{d\,\mathbf{y_{ERR}}(t_{k+1})_m}{d\,\mathbf{u_{ERR}}(t_k)_m} \tag{11}$$

where,

$$\mathbf{u_{ERR}}(t_k)_m = \mathbf{u}(t_k)_m - \mathbf{u_{DES}}(t_k) \tag{12}$$

so equation (10) can be rewritten as shown in (13).

$$[\mathbf{J}]\,\mathbf{u_{ERR}}(t_k)_m = \mathbf{y_{ERR}}(t_{k+1})_m \tag{13}$$

The next estimate in the Newton-Raphson iteration is evaluated using a modified form of equation (7) :

$$\mathbf{u}(t_k)_{m+1} = \mathbf{u}(t_k)_m - \mathbf{u_{ERR}}(t_k)_m. \tag{14}$$

For the case where the number of constraints and controls are equal, Crout's Factorisation Method [3] allows an exact solution of (13) for $\mathbf{u_{ERR}}(t_k)_m$. The modified algorithm has been tested for such a case and gives exactly the same results as the method in §1.2. Alternatively if the number of controls exceeds the number of constrained states it is possible, using Singular Value Decomposition, to find a Least Squares minimal solution [4] for $\mathbf{u_{ERR}}(t_k)_m$. Thus using this algorithm a flight path parameter can be left undefined and an optimal solution evaluated for the remaining constraints. Figure 1 presents the algorithm in the form of a flowchart.

2. Verification of the CSM

To ensure that the CSM Fortran was in a form consistent with *Genisa*, it was written from model documentation rather than transporting the existing code directly. The equations of motion contain Euler rotational expressions - (18), (19), (20) -

which, due to the transfer functions used, are peculiar to the CSM . In addition to the six Euler, three kinematic and three Euler transformation equations are three for the actuator states. Equations (15) to (26) are more specific representations of (1).

Three translational and three rotational Euler rigid body equations :

$$\dot{u}_B = -(w_B q - v_B r) + \frac{X}{m} + g \sin\theta \tag{15}$$

$$\dot{v}_B = -(u_B r - w_B p) + \frac{Y}{m} - g \cos\theta \sin\phi \tag{16}$$

$$\dot{w}_B = -(v_B p - u_B q) + \frac{Z}{m} - g \cos\theta \cos\phi \tag{17}$$

$$\dot{p} = -L_p (\eta_{1c} + p_{DEM_{TC}} - p) \tag{18}$$

$$\dot{q} = M_{TC} - M_q (\eta_{1s} + q_{DEM_{TC}} - q) \tag{19}$$

$$\dot{r} = N_{TC} - N_r (\eta_{0TR} + 2.0\,\dot{\beta} - N_r \beta). \tag{20}$$

Three kinematic relations :

$$\dot{\phi} = p + q \sin\phi \tan\theta + r \cos\phi \tan\theta \tag{21}$$

$$\dot{\theta} = q \cos\phi - r \sin\phi \tag{22}$$

$$\dot{\psi} = q \sin\phi \sec\theta + r \cos\phi \sec\theta. \tag{23}$$

Three actuator states :

$$\dot{\eta}_{1s} = \frac{q_{DEM} - \eta_{1s}}{\tau_a} \tag{24}$$

$$\dot{\eta}_{1c} = \frac{p_{DEM} - \eta_{1c}}{\tau_a} \tag{25}$$

$$\dot{\eta}_{0TR} = \frac{r_{DEM} - \eta_{0TR}}{\tau_a}. \tag{26}$$

The earth fixed velocities $\dot{x}_E$, $\dot{y}_E$ and $\dot{z}_E$ can be calculated from the translational body fixed velocities u_B, v_B and w_B and the attitude angles ϕ, θ and ψ by the Euler transformation equations where the transformation matrix $[l_1, \ldots, n_3]$ is effectively the function **g** in equation (2).

$$\begin{bmatrix} \dot{x}_E \\ \dot{y}_E \\ \dot{z}_E \end{bmatrix} = \begin{bmatrix} l_1 & m_1 & n_1 \\ l_2 & m_2 & n_2 \\ l_3 & m_3 & n_3 \end{bmatrix} \begin{bmatrix} u_B \\ v_B \\ w_B \end{bmatrix} \tag{27}$$

$$l_1 = \cos\theta \cos\psi$$
$$l_2 = \cos\theta \sin\psi$$
$$l_3 = -\sin\theta$$
$$m_1 = \sin\phi \sin\theta \cos\psi - \cos\phi \sin\psi$$
$$m_2 = \sin\phi \sin\theta \sin\psi + \cos\phi \cos\psi$$
$$m_3 = \sin\phi \cos\theta$$
$$n_1 = \cos\phi \sin\theta \cos\psi + \sin\phi \sin\psi$$
$$n_2 = \cos\phi \sin\theta \sin\psi - \sin\phi \cos\psi$$
$$n_3 = \cos\phi \cos\theta$$

Before attempting inverse simulation, it was necessary to compare the responses of the DRA and *Genisa* CSM models during conventional simulation. Small inconsistencies were considered allowable as the models differ slightly; for example the inclusion of a Z_{FUS} force and tailplane model in the DRA version. Configurational data is given in Appendix B. Firstly a comparison was made between the respective trim conditions over a range of velocities, and then the control responses were verified. The next section describes the method by which *Genisa* trims the CSM.

2.1 Trim

Due to the decoupled nature of the CSM, steady level flight is characterised by the attitudes ϕ and ψ and the directional controls η, ξ and ζ being equal to zero. The equations of motion are thus reduced to four in terms of unknowns u_B, v_B, θ and δ_C depending upon the flight velocity. Trim is found by a Newton-Raphson solution of equations (28) to (31),

$$X_{TOT} - m\,g\sin\theta = 0 \tag{28}$$

$$Z_{TOT} = m\,g\cos\theta = 0 \tag{29}$$

$$V_T - u_B \cos\theta - w_B \sin\theta = 0 \tag{30}$$

$$- u_B \sin\theta + w_B \cos\theta = 0 \tag{31}$$

$$X_{TOT} = X_{ROT}(u_B, w_B, \delta_C) + X_{FUS}(u_B, w_B) \text{ and } Z_{TOT} = Z_{ROT}(u_B, w_B, \delta_C)$$

Comparisons of θ (V_T) and δ_C (V_T) for the two models are shown in Figures 2 and 3.

The correlation is good, differences accountable for by discrepancies in the modelling and trim algorithm (DRA solves for α, θ, δ_C). The second test is to compare model responses to prescribed control inputs.

2.2 Responses to Step Inputs of η, ξ and ζ

This paper concentrates on the Lateral Jinking manoeuvre and it is therefore appropriate to verify the CSM response to roll inceptor, ξ. Figure 4 illustrates the (*Genisa*) CSM response to a 1 second step input of ξ.

The results shown in Figure 4 and others for η and ζ compare well with data documented at DRA Bedford and are consistent with the form of a first over, second order system. The CSM used within *Genisa* appears to perform accurately.

3. Inverse Simulation Incorporating the CSM

With inverse simulation of a conventional helicopter model, one common approach is to demand that the helicopter adheres to the manoeuvre flight path velocities, $\dot{x}_E$, $\dot{y}_E$ and $\dot{z}_E$ and heading rate $\dot{\psi}$ [1]. Initial studies however, where the helicopter was simply constrained to maintain trim, indicate that this is not possible using the CSM. Investigation of results shows that although $\dot{z}_E$ and $\dot{\psi}$ respond favourably to collective and yaw inputs (δ_C and ζ), the longitudinal and lateral velocities are very insensitive to inputs of pitch and roll (η and ξ). These inputs have a significant effect over several seconds, but over a typical integration interval (0.1 sec) the relevant Jacobian elements are much smaller than those differentiated with respect to δ_C. Experimentation has shown that by constraining $\dot{z}_E$ and either the angular body velocities q, p, r or attitude rates $\dot{\theta}$, $\dot{\phi}$ and $\dot{\psi}$ the algorithm does succeed in maintaining trim. The reasons for this become apparent if the CSM controls are compared with those of a conventional helicopter model. In a multiblade model,

longitudinal and lateral cyclic inputs (θ_{1s} and θ_{1c}) tilt the rotor disc which alters the direction of the thrust vector, changing forces and so directly affecting the translational states. Due to the offset of the vector from the centre of gravity, moments are produced and angular states are also affected directly. By contrast CSM responses to the pitch and roll inceptors, η and ξ (which are analogous to the cyclic controls) are modelled using transfer functions relating them to the angular rates q and p. With no coupling between the angular and translational states, $\dot{x}_E$ and $\dot{z}_E$ are affected only indirectly once q and p have changed significantly. This explains the discrepancy between the immediate and longer term translational state responses. Any manoeuvres to be used for inverse simulation of the CSM must be defined in terms of angular parameters.

The manoeuvre used to produce the results in this report was Lateral Jinking as described in the next section.

3.1 The Lateral Jinking (LJ) Manoeuvre

Lateral Jinking, hencewith referred to as LJ is defined by DRA Bedford to represent transient turning and tracking in low level NOE flight. The primary control axis is roll. Typically the aircraft is initially in forward flight at 60 kts and 7.5 m altitude. It is subsequently displaced laterally by 23 m (at the very least 16 m) to the left and stabilised on a parallel track for 6 secs, then returned to the original heading and groundtrack. Figure 5 summarises the groundtrack.

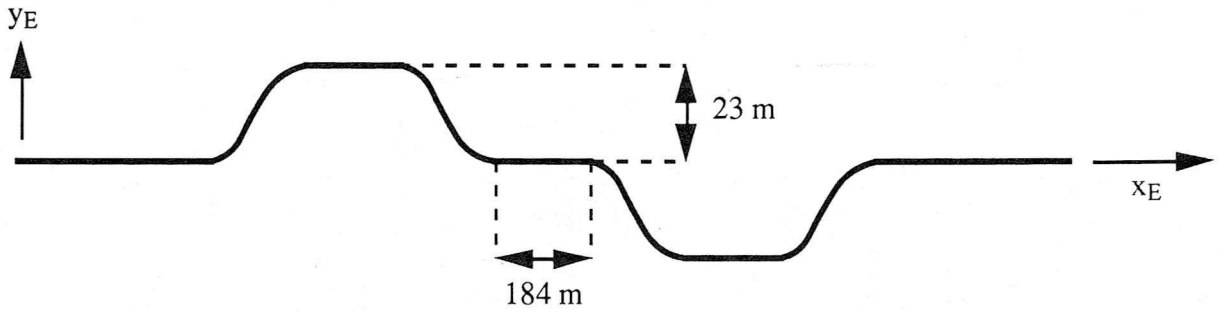

Figure 5 **Groundtrack for Lateral Jinking Manoeuvre**

When flying the manoeuvre pilots are given the following guidelines.

1. Endeavour to maintain an approximately symmetrical roll attitude profile when 'rolling in' and 'rolling out'.

2. Within the constraints of desired levels of aggression (ϕ_{MAX} equal to 15°, 30° or 45°), minimise the time between tracking phases.

3.2 Lateral Jinking Applied to the CSM

As discussed at the beginning of §3, the manoeuvre must be defined in terms of angular parameters and altitiude. The chosen states are $\dot{\theta}$ (t), $\dot{\phi}$ (t), $\dot{\psi}$ (t) and $\dot{z}_E$ (t) which are controlled respectively by the pitch (η), roll (ξ) and yaw (ζ) inceptors and collective (δ_C). DRA guidelines, §3.1, demand a constant altitude of 7.5 m and a true balanced turn which will displace the helicopter 23 m laterally. Analysis of AFS (Advanced Flight Simulator) results indicate that the manoeuvre is controlled by the roll inceptor, ξ and that the CSM turn coordination augmentations allow a true balanced turn consistent with a zero-sideslip condition. The constraints are thus defined as follows.

i) Vertical Velocity, $\dot{z}_E$ (t)

To ensure that the helicopter is kept at a constant altitude of 7.5 m, the vertical velocity is constrained to be zero.

$$\dot{z}_E (t) = 0$$

ii) Pitch Rate, $\dot{\theta}$ (t)

As the flight velocity is constant and there is no coupling between pitch and roll it is possible to demand a steady 60 kts trim pitch setting, thus $\dot{\theta}$ (t) is set to zero.

$$\dot{\theta} (t) = 0$$

iii) Bank Rate, $\dot{\phi}$ (t)

The demanded time history of $\dot{\phi}$ (t) controls the helicopter during the manoeuvre. Figure 6 shows an idealised representation of a typical DRA AFS bank angle response during a LJ manoeuvre. The vehicle, originally at zero bank, is rolled into the turn to a bank limit of - ϕ_{MAX} by a pulse of roll inceptor (the profile of which is similar to that of $\dot{\phi}$ (t)) and then back to zero at the turn mid-point. It is then rolled out of the turn up to + ϕ_{MAX} and back to zero in time for the next straight. This ensures that the helicopter accelerates laterally into the bend to a maximum value of

$\dot{y}_E$ (t) and decelerates out so that the lateral velocity is equal to zero as the helicopter enters the straight. The boundary conditions for ϕ (t) and resultant polynomial for $\dot{\phi}$ (t) are detailed in §3.3.

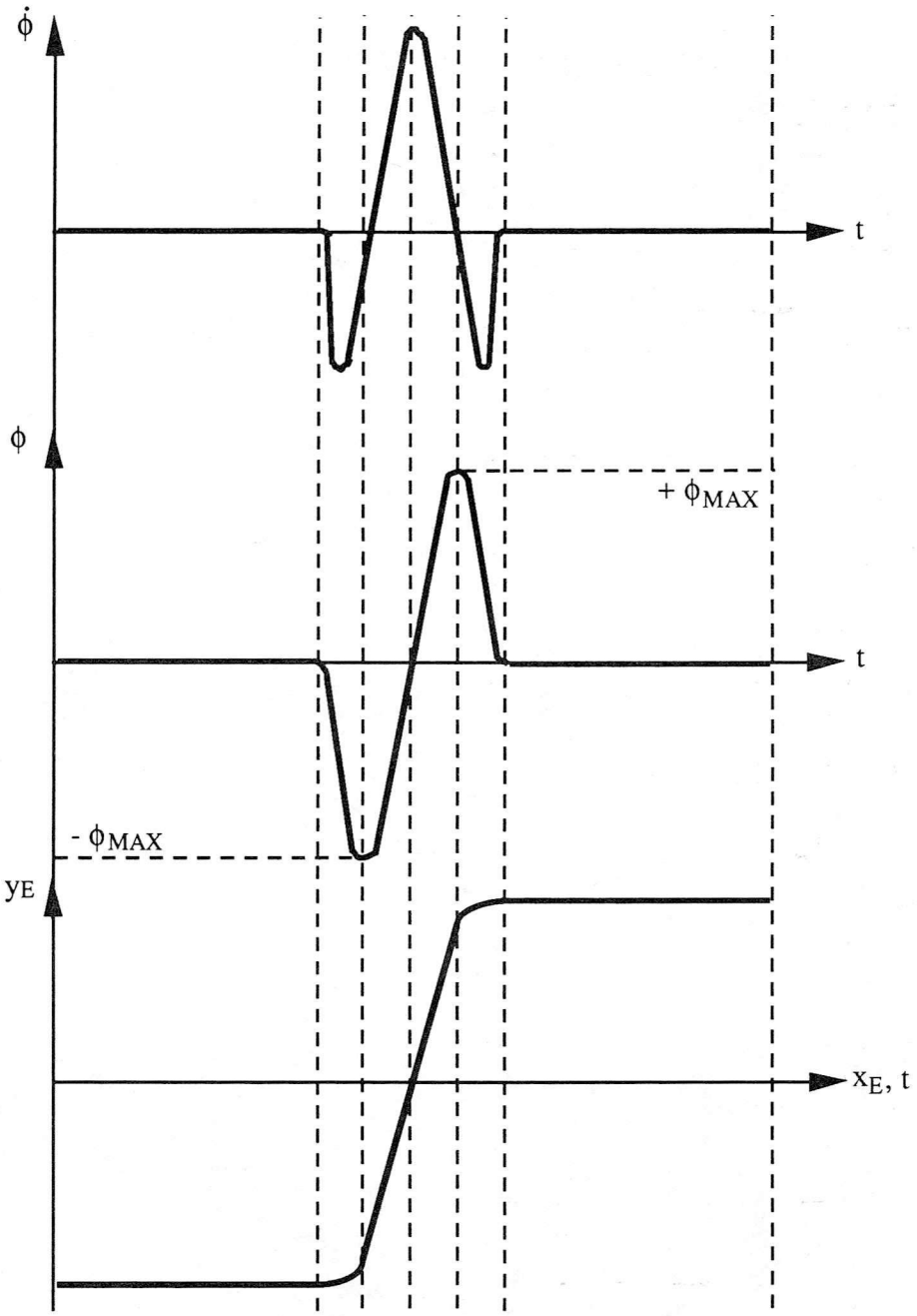

Figure 6 **Bank Rate, Bank Angle and Groundtrack During Transient Turn**

iv) Yaw Rate, $\dot{\psi}$ (t)

The heading angle should be such as to produce a true balanced turn and maintain zero-sideslip consistent with weathercock stability. Given a constant pitch

angle, θ_e the turn coordination terms calculate a suitable value for heading angle, ψ (t) as a function of the instantaneous bank angle, ϕ (t).

As it is unnecessary to define a yaw rate time history, $\dot{\psi}$(t), the manoeuvre can be fully described by the states $\dot{z}_E$ (t), $\dot{\theta}$ (t) and $\dot{\phi}$ (t). The result is 4 controls, 3 constrained states and consequently a rectangular Jacobian. Referring to §1.3, the algorithm can solve such a problem by finding a Least Squares minimisation of equation (13). A more detailed representation of (13) is presented as equation (32) below.

$$\begin{bmatrix} \frac{\partial \dot{z}_E}{\partial \delta_C} & \frac{\partial \dot{z}_E}{\partial \eta} & \frac{\partial \dot{z}_E}{\partial \xi} & \frac{\partial \dot{z}_E}{\partial \zeta} \\ \frac{\partial \dot{\theta}}{\partial \delta_C} & \frac{\partial \dot{\theta}}{\partial \eta} & \frac{\partial \dot{\theta}}{\partial \xi} & \frac{\partial \dot{\theta}}{\partial \zeta} \\ \frac{\partial \dot{\phi}}{\partial \delta_C} & \frac{\partial \dot{\phi}}{\partial \eta} & \frac{\partial \dot{\phi}}{\partial \xi} & \frac{\partial \dot{\phi}}{\partial \zeta} \end{bmatrix} \begin{bmatrix} \delta_C - \delta_{C\,DES} \\ \eta - \eta_{DES} \\ \xi - \xi_{DES} \\ \zeta - \zeta_{DES} \end{bmatrix} = \begin{bmatrix} \dot{z}_E - \dot{z}_{E\,DES} \\ \dot{\theta} - \dot{\theta}_{DES} \\ \dot{\phi} - \dot{\phi}_{DES} \end{bmatrix} \qquad (32)$$

3.3 Definition of Bank Rate Time History, $\dot{\phi}$ (t)

The bank angle time history ϕ (t), shown in Figure 7, can be described by four sections within the interval OE.

i) OA : time to maximum negative bank, t_1

This section is defined by six boundary conditions :

O : $\phi = 0, \dot{\phi} = 0, \ddot{\phi} = 0$

A : $\phi = -\phi_{MAX}, \dot{\phi} = 0, \ddot{\phi} = 0$

which determine the coefficients for a 5th order polynomial of ϕ (t)

$$\phi(t) = \left[-10 \left(\frac{t}{t_1}\right)^3 + 15 \left(\frac{t}{t_1}\right)^4 - 6 \left(\frac{t}{t_1}\right)^5 \right] \phi_{MAX}$$

and, by differentiation, a 4th order polynomial for $\dot{\phi}$ (t)

$$\dot{\phi}(t) = \left[- \left(\frac{t}{t_1}\right)^2 + 2 \left(\frac{t}{t_1}\right)^3 - \left(\frac{t}{t_1}\right)^4 \right] \frac{30\,\phi_{MAX}}{t_1}. \qquad (33)$$

ii) AB : time at maximum negative bank, t_2

As the bank angle is a constant value of - ϕ_{MAX}, the bank rate is clearly equal to zero.

$$\dot{\phi}\,(t) = 0$$

iii) BC : time from maximum negative to maximum positive bank, 2 t_1

Six boundary conditions :

B : $\phi = -\phi_{MAX}, \dot{\phi} = 0, \ddot{\phi} = 0$
C : $\phi = +\phi_{MAX}, \dot{\phi} = 0, \ddot{\phi} = 0$

allow definition of a 4th order polynomial for bank rate, $\dot{\phi}\,(t)$

$$\phi\,(t) = \left[\, 4\left(\frac{t}{t_1}\right)^2 - 4\left(\frac{t}{t_1}\right)^3 + \left(\frac{t}{t_1}\right)^4 \right] \frac{15\,\phi_{MAX}}{8\,t_1}. \qquad (34)$$

iv) DE : time at zero bank, t_3

During the period of the manoeuvre straight, bank angle $\phi\,(t)$ and thus rate are equal to zero.

$$\dot{\phi}\,(t) = 0$$

All other sections of the manoeuvre can be expressed as positive or negative values of i) → iv). For example the polynomial for EF is described by changing the signs of equation (33).

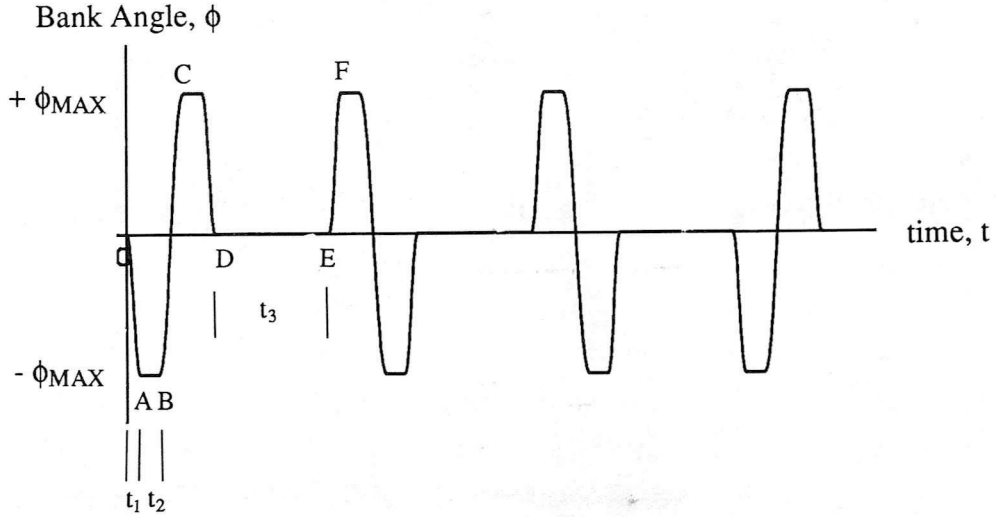

Figure 7 **Bank Angle Time History**

3.4 Manoeuvre Periods

The final manoeuvre shape is controlled by the periods t_1 and t_2, which are dependent upon the choice of roll derivative, L_p and level of aggression ϕ_{MAX}.

i) t_1 Roll acceleration. Referring to Figure 4 it is possible to estimate the time taken to achieve ϕ_{MAX} for a unit step of roll inceptor. Such response plots indicate the minimum allowable value for t_1 which will not exceed the control limit ($\xi_{MAX} = \pm 1$) in inverse simulation. The minimum value of t_1 is proportional to the roll derivative, L_p.

ii) t_2 A value must be chosen which produces the desired lateral displacement. To obtain the displacement requires running the full *Genisa* algorithm, which implies repeated calculations until an appropriate value of t_2 is found. This would be computationally expensive so values were established by trial and error. In addition the determined values of t_1 are only guidelines which devalues accurate calculations of t_2. If inverse simulation of the CSM is to be used as a future control design tool, it is assumed that a qualitative understanding of how constraints such as $\dot{\phi}$ (t) affect a system are of more importance than fixed numerical accuracy. Such a trial and error procedure is desirable as it avoids dependence between the inverse algorithm and the manoeuvre thus allowing the designer more flexibility.

iii) t_3 The manoeuvre specification suggests 6 secs for the straight section. This is to allow any characteristic oscillations to damp down.

4. Results

All results produced here are for the LJ manoeuvre described in §3. Vehicle responses, control inputs and flight paths are included for two cases reflecting different aggression parameters. Both manoeuvres attempt to minimise the time taken to displace 23 m laterally but being constrained to either 15° or 45° bank the result are substantially different, albeit with qualitative similarities. By contrast with inverse simulation results produced using a conventional model, [1], it cannot be assumed that the vehicle will adhere closely to the desired flight path as this is not defined explicitly. Though the algorithm did match the desired attitudes very closely and ensure a small sideslip, it became apparent during the course of running tests that a groundtrack of any accuracy needs careful choice of time step and appreciation of manoeuvre severity. As shown in Appendix B all gains are unity and the derivatives L_p, M_q and N_r are equal to - 9.0, - 4.5 and - 4.5 respectively.

4.1 Accuracy of Results

Case 1 : low aggression parameter; $\phi_{MAX} = 15°$. As a unit step input is the maximum allowable control displacement, Figure 4 indicates the minimum time required for the helicopter to bank to ± 15°; approximately 0.28 secs. Using this value of t_1 and a non-specific t_2, the controls did indeed reach, but not exceed, the control boundary. The resultant groundtrack, however, was poor as the algorithm was unable to achieve zero bank and heading in preparation for the straights, and the helicopter drifted off track. Various combinations of t_1 and t_2 were tried in an effort to find values which maintained a reasonable track and produced a lateral displacement close to 23 m. Thus t_1, t_2 and t_3 in results for Case 1 are equal to 0.5, 2.2 and 6.0 seconds respectively.

Case 2 : high aggression parameter; $\phi_{MAX} = 45°$. Similarly to Case 1, the estimated value of t_1 (0.56 sec) resulted in an inaccurate flight path. The values chosen were 1.0, 0.1 and 6.0 seconds respectively. Clearly the model requires longer to achieve 45° rather than 15° bank, but much less time need be spent at ϕ_{MAX} to produce the same displacement.

Plots for Cases 1 and 2 are presented in Figures 8, 9, 10 and 11, all of which show good results. As expected the maximum lateral control displacement, ξ is close to ± 1 reflecting the demanded bank rate. The other three controls are, by comparison, very close to trim. Altitude and pitch and bank attitudes, which are of course constrained, are very close to the prescribed values; θ and z_E remaining at their trim levels and ϕ matching the intended profile. Comparing Figure 9 with 6 and 7 confirms the good correlation. The length of plateaux in Case 1 reflect how much longer the helicopter must adopt maximum bank than in Case 2 where the time spent at 45° shows as little more than a peak. The different profiles are of course accounted for by contrasting the appropriate values of t_1 and t_2. Of interest are the unconstrained heading responses, ψ, both of which attempt a no sideslip condition in response to the instantaneous bank angle by holding the flight velocity vector in the body x_B-z_B plane. Both the least squares minimisation and the CSM turn coordination terms are influential in this adopted configuration which, as mentioned earlier, agrees with weathercock stability. The small sideslip and pitch angles are confirmed by the domination of u_B over the other translational velocity terms v_B and w_B. Roll rate, p is of a form similar to ξ: accordingly the yaw rate profile matches that of the heading angle, and the fluctuations in the collective and longitudinal inputs reappear in the longitudinal state responses w_B and q. The helicopter's freedom about the yaw axis is

apparent from the lack of restraining pedal input, ζ. All the results show good correlation with data from DRA simulations.

4.2 Drift from Desired Groundtrack

As the bank angle time history profile is a combination of functions rather than one continuous polynomial it is important to choose a time step which will adequately capture the transition phase. If this is not satisfied then subsequent sections suffer from bad initial conditions and, as mentioned above, the vehicle drifts off track. This problem is accentuated by increasing manoeuvre severity, characterised by a small t_1, as a high rate of change of ϕ will add to the probability of maxima / minima passing between time points. The result of this is failure to secure zero bank at the start of a straight section, causing drift. An example of such a groundtrack is shown as Case 3 on Figure 10 where ϕ_{MAX}, t_1 and t_2 are equal to 45°, 0.5 and 0.8 secs respectively.

5. Conclusions and Recomendations

1. There is good correlation between the responses of the CSM written for *Genisa* and the version used at DRA Bedford.

2. For successful inverse simulation of the CSM it is not possible to define manoeuvres in terms of flight path parameters. Because of the peculiar nature of the controls, constraints must be described in terms of vehicle body angular velocities or attitude rates.

3. As the desired flight path is not defined explicitly, its accuracy is not guaranteed. With the relationship between controls and angular responses, however, it is possible to avoid exceeding control limits. This means that the manoeuvre can always be flown regardless of how it matches the expected profile.

4. Good choice of inputs produces very accurate manoeuvres and smooth, realisable vehicle responses for all but the most severe demands. In addition the results compare very favourably with those recorded on the Advanced Flight Simulator at DRA Bedford.

5. The advantages of the Conceptual Simulation Model, which assumes full decoupling via an active control system, are evident in the inverse simulation results. The Lateral Jinking manoeuvre can be flown using almost exclusively one control;

the lateral input or roll inceptor, ξ. This directly affects the roll rate, p and consequently the bank angle ϕ, the time history of which itself describes LJ. Using the least squares minimisation mentioned in §1.3 it is possible to demand constant pitch, θ without adversely affecting other states as the CSM turn coordination terms ensure a heading, ψ consistent with a no-sideslip condition.

5. For the reasons detailed in 3. and 4. *GenisaCSM* is potentially a useful design tool for either minimising pilot effort or maximising vehicle performance.

6. *GenisaCSM* could well be used for other manoeuvres though, as here, with careful consideration of the task and subsequent user inputs.

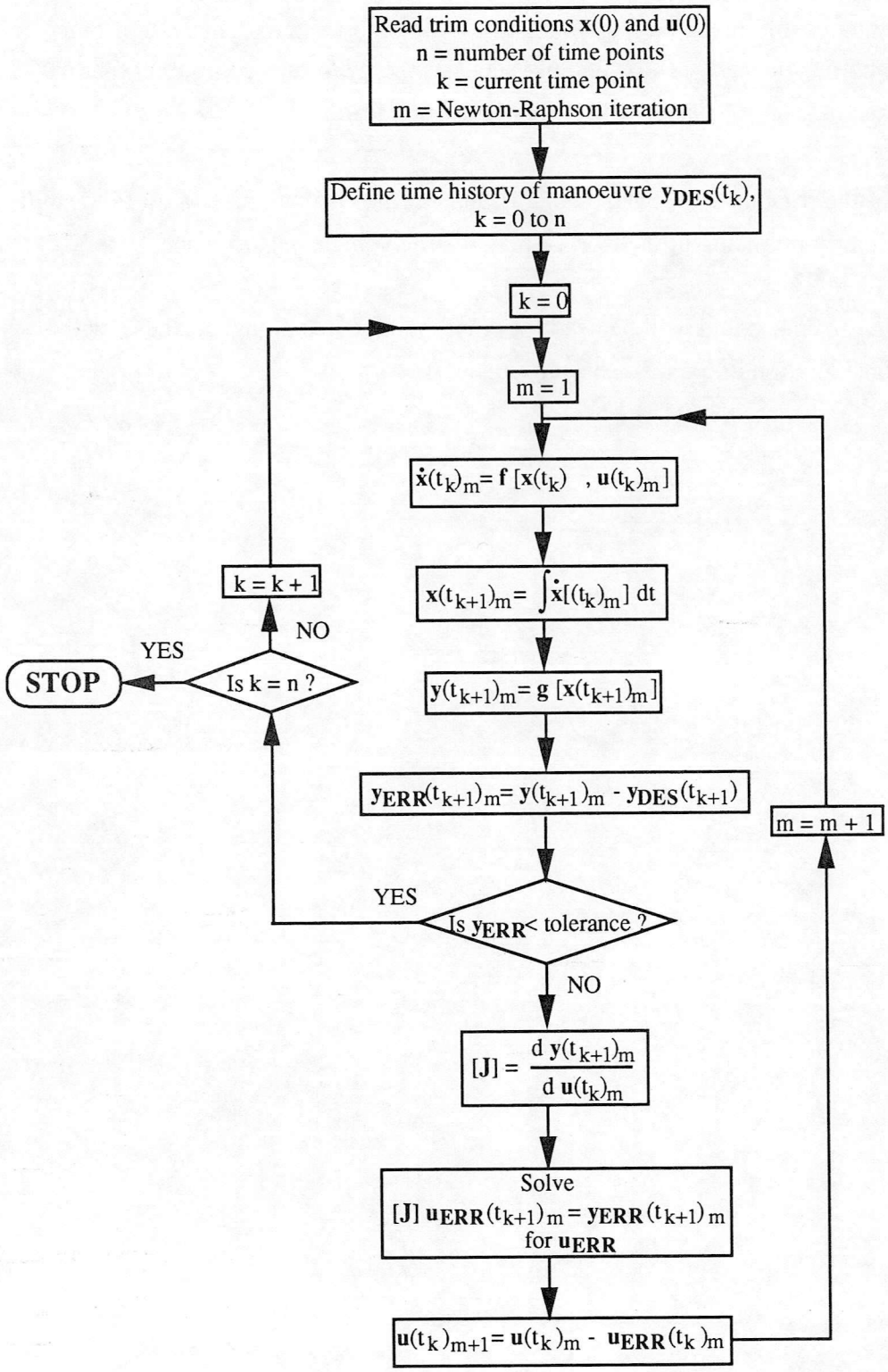

Figure 1 **Flowchart for the Generic Inverse Simulation Algorithm**

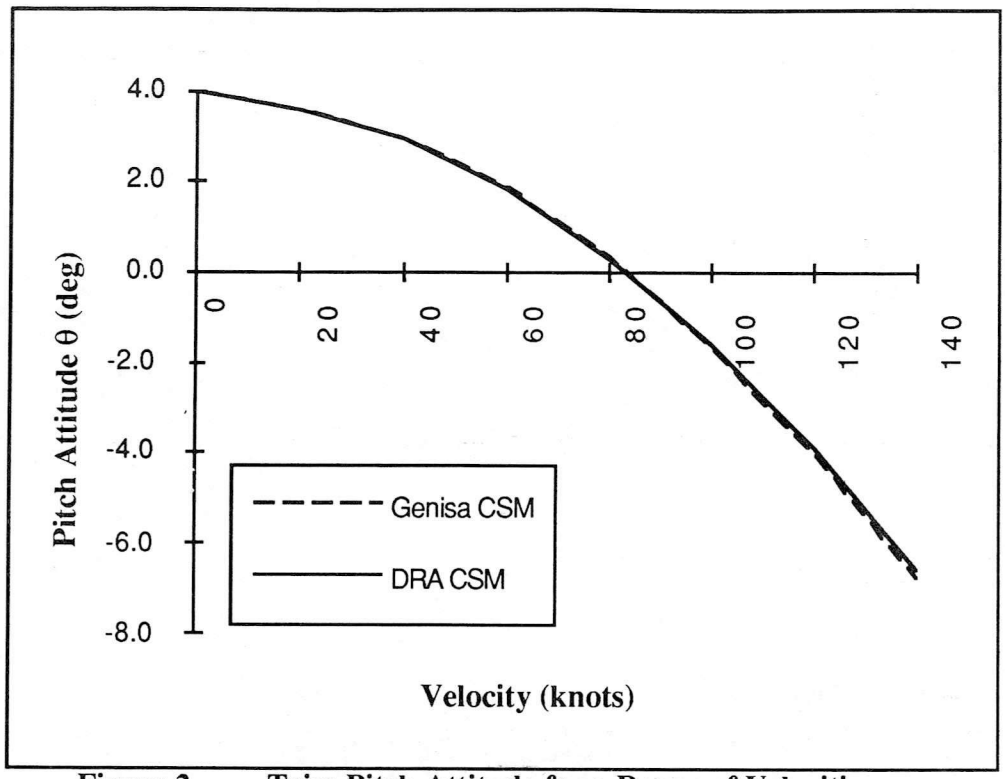

Figure 2 Trim Pitch Attitude for a Range of Velocities

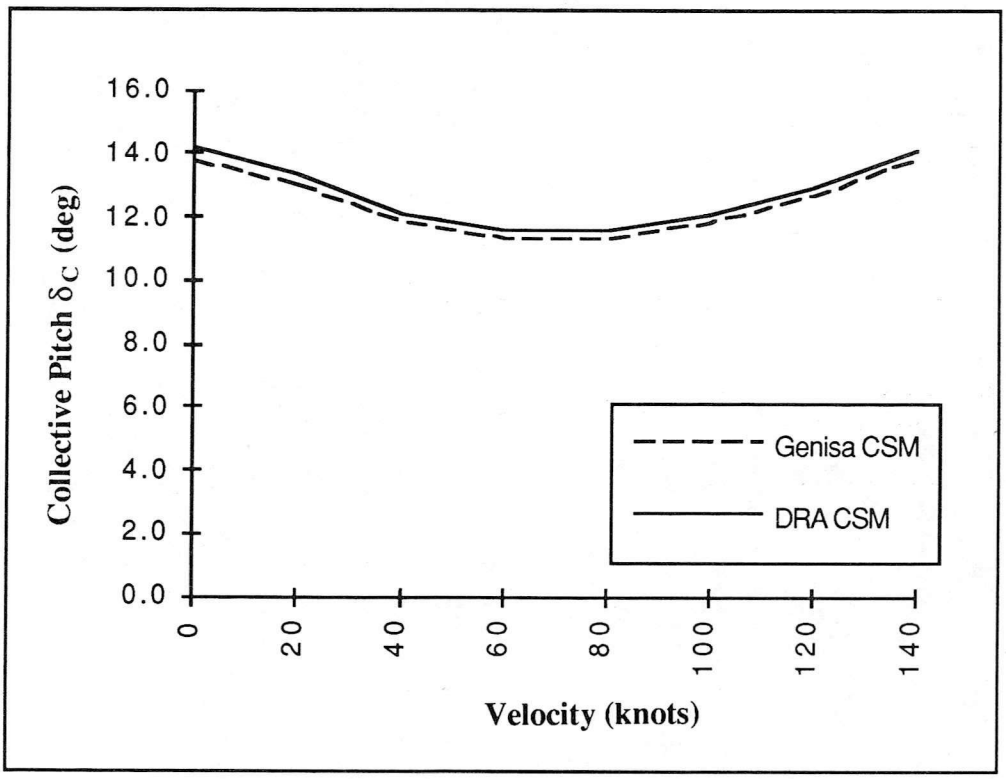

Figure 3 Trim Collective Pitch Input for a Range of Velocities

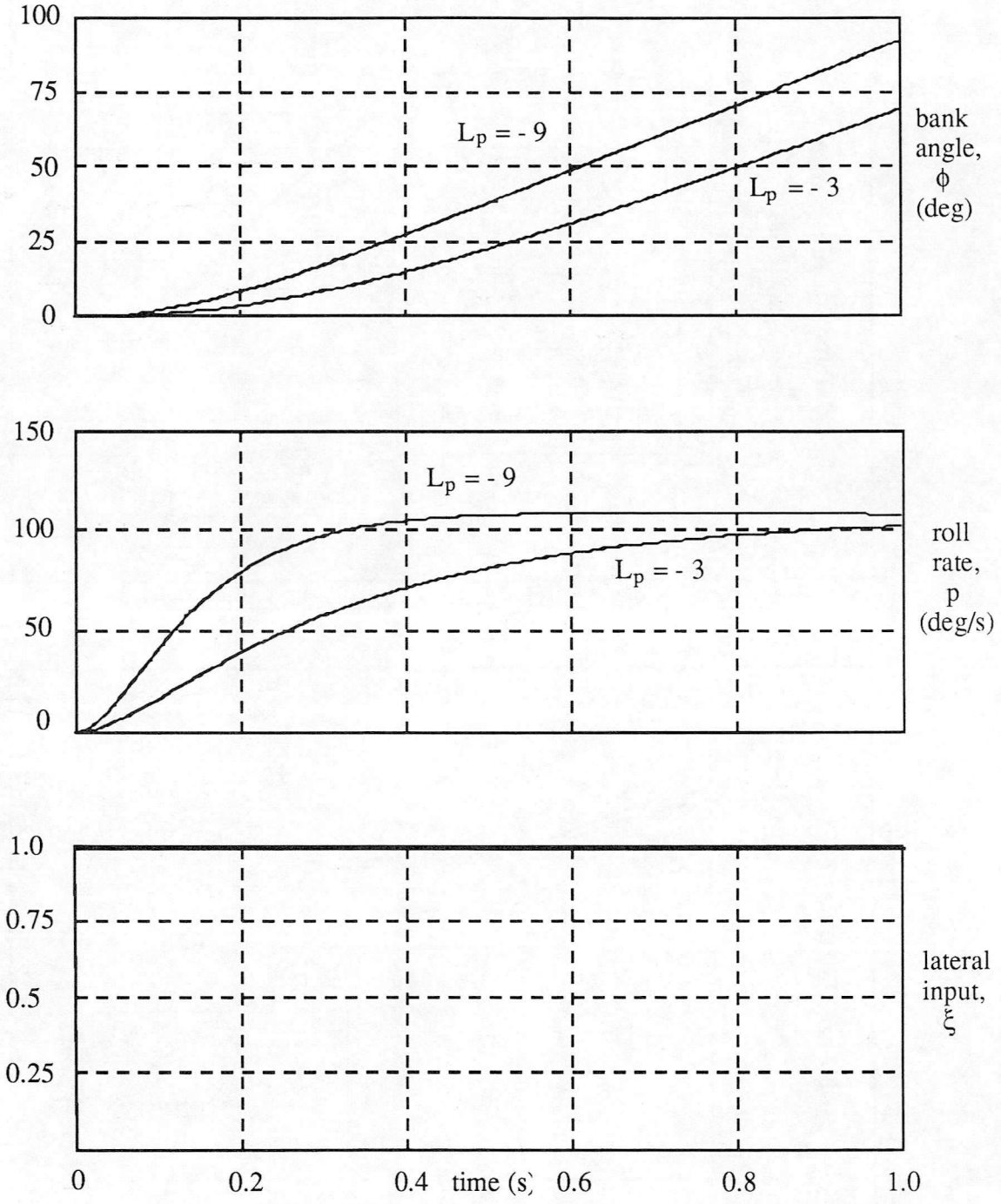

Figure 4 **CSM Roll Response to a Unit Step Input, ξ**

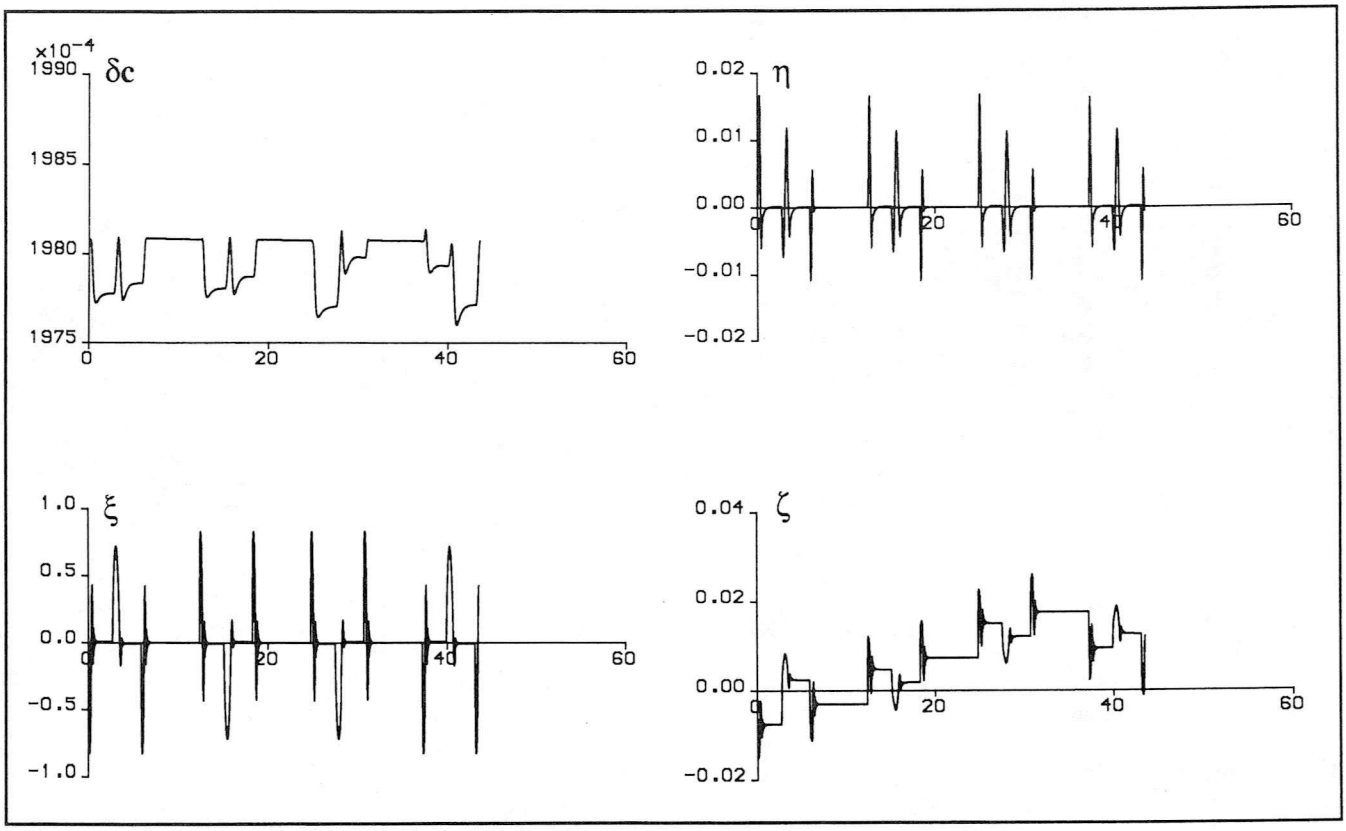

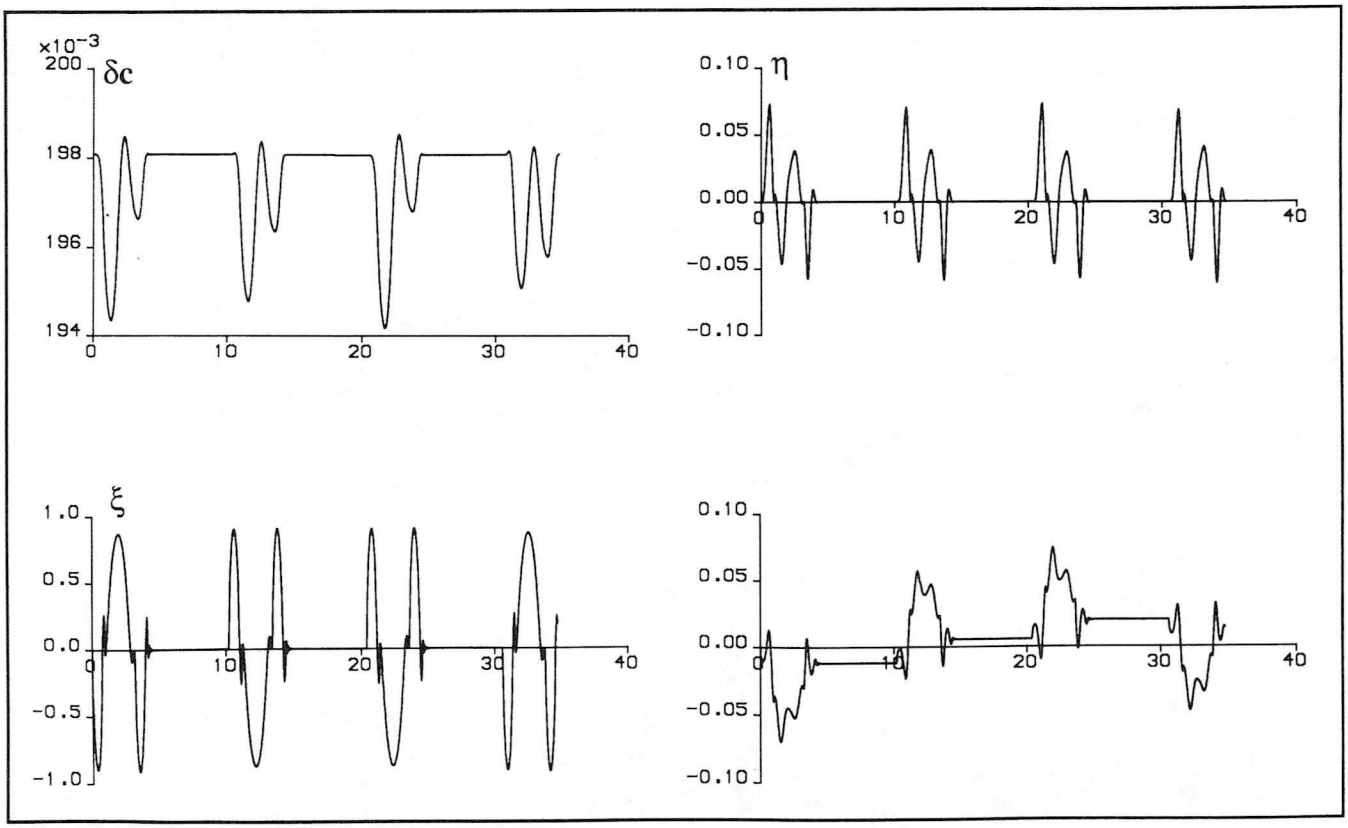

Figure 8 Control Inputs Calculated by *Genisa* for Case 1 (upper) and Case 2 (lower) δc, η, ξ and ζ vs. time (secs)

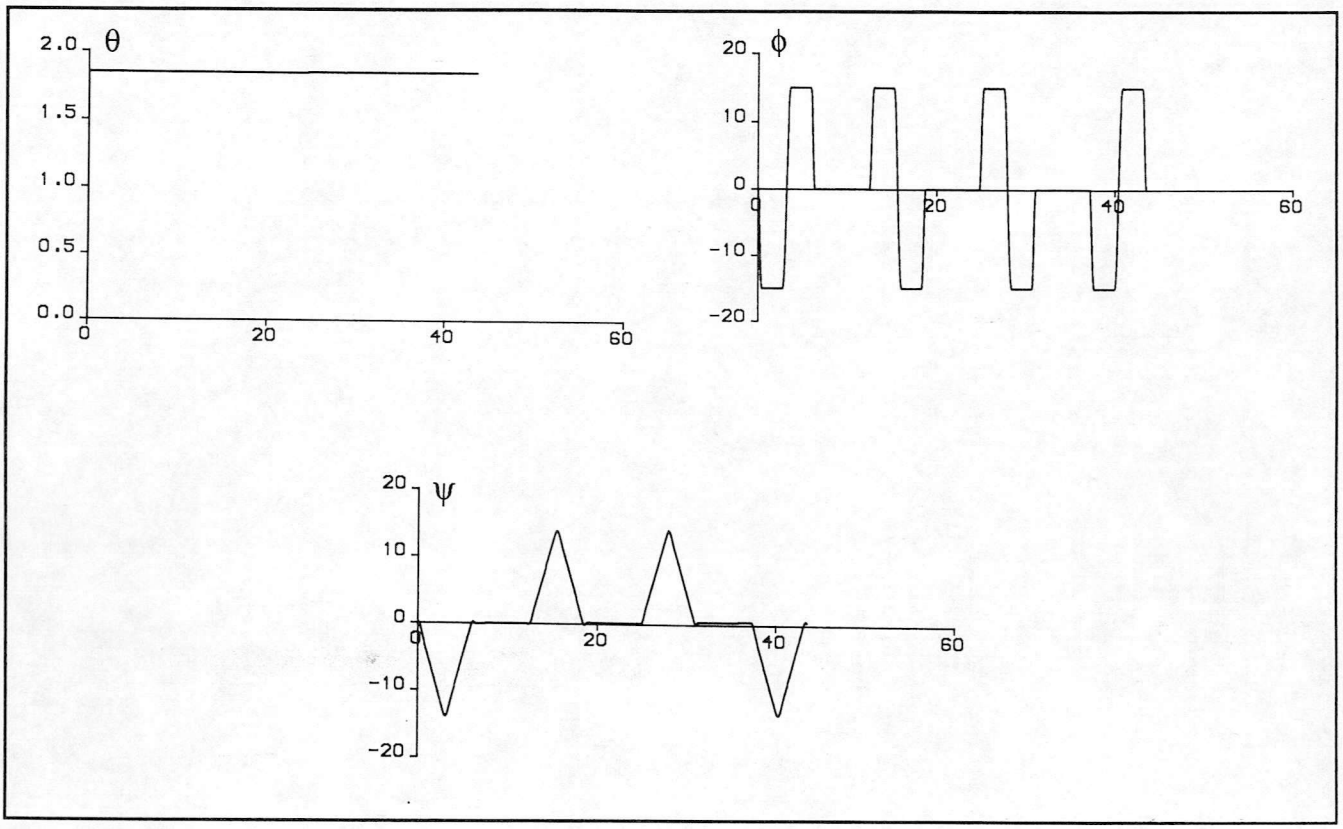

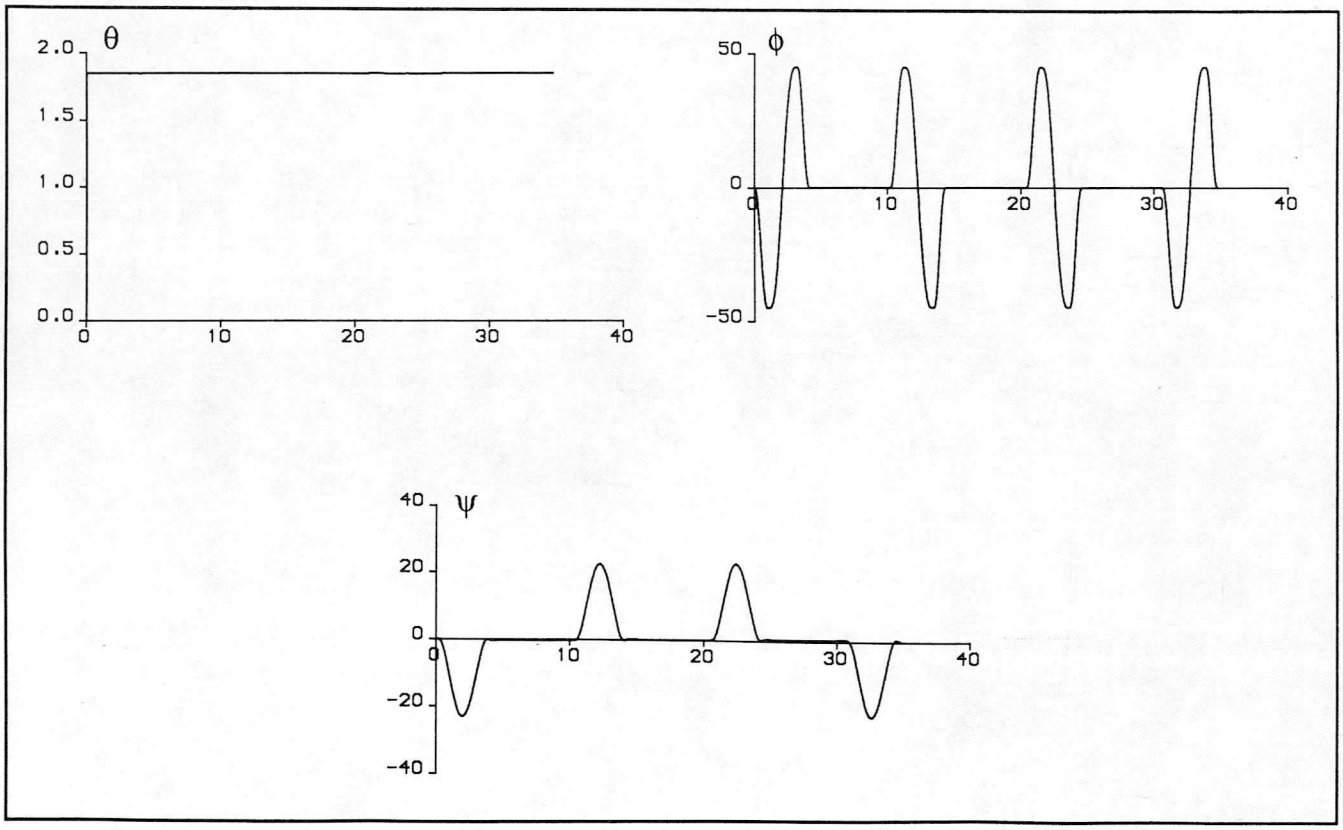

Figure 9 **Attitude Angles Calculated by *Genisa* for Cases 1 and 2**
θ, ϕ and ψ (deg) vs. time (secs)

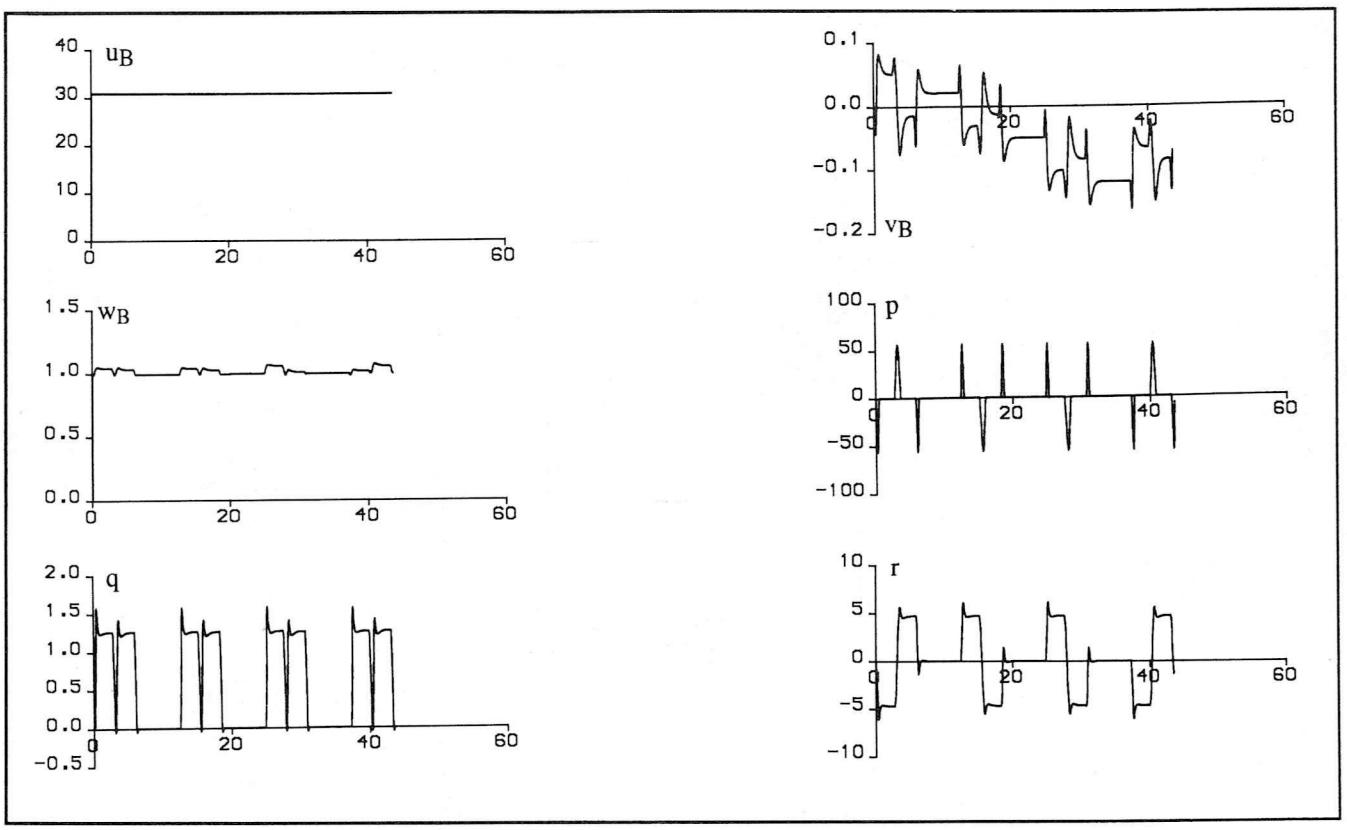

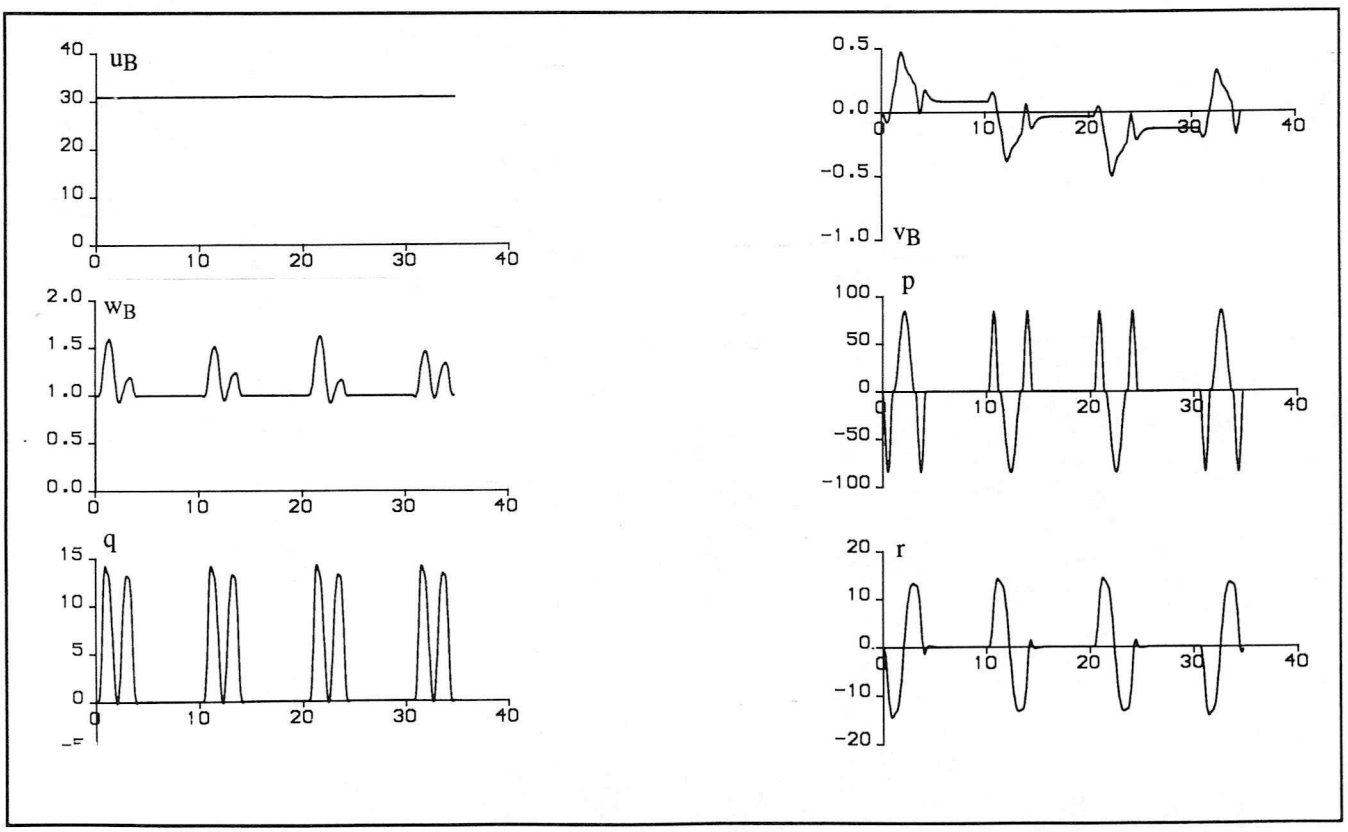

Figure 10 **Body Velocities Calculated by *Genisa* for Cases 1 and 2**
u_B, v_B and w_B (m/s) and p, q and r (deg/s) vs. time (secs)

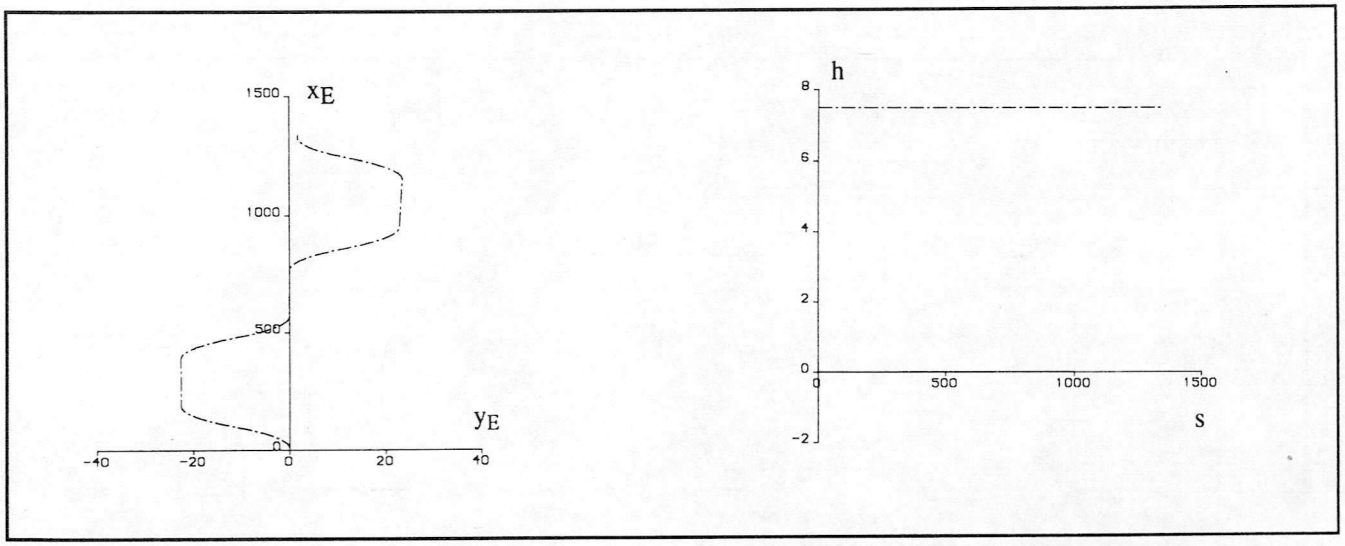

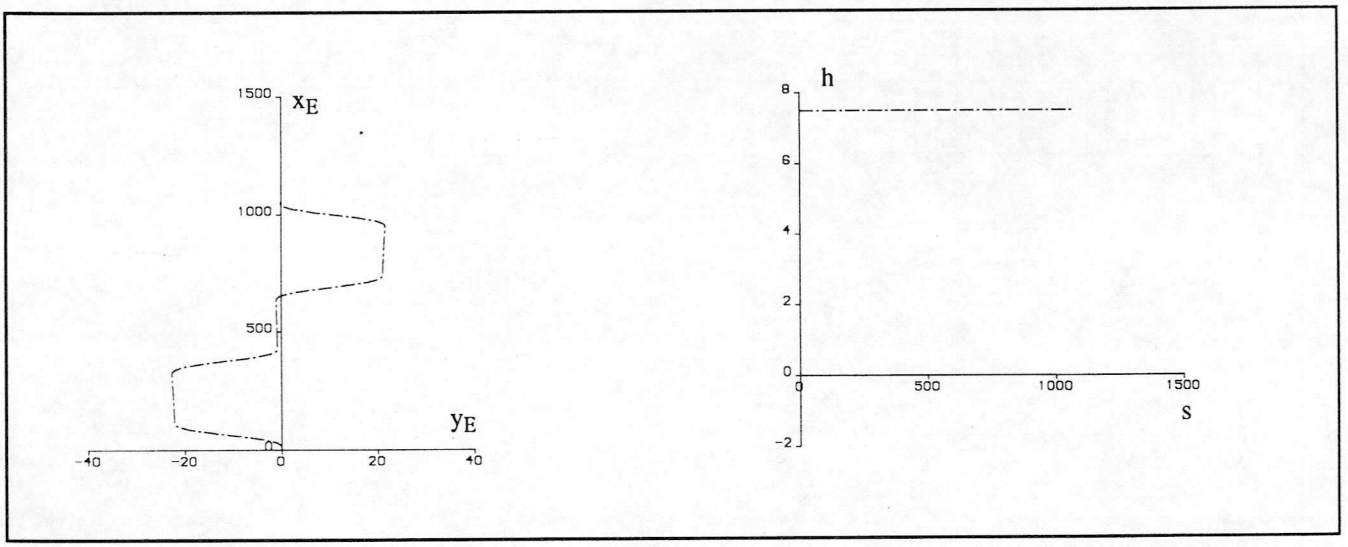

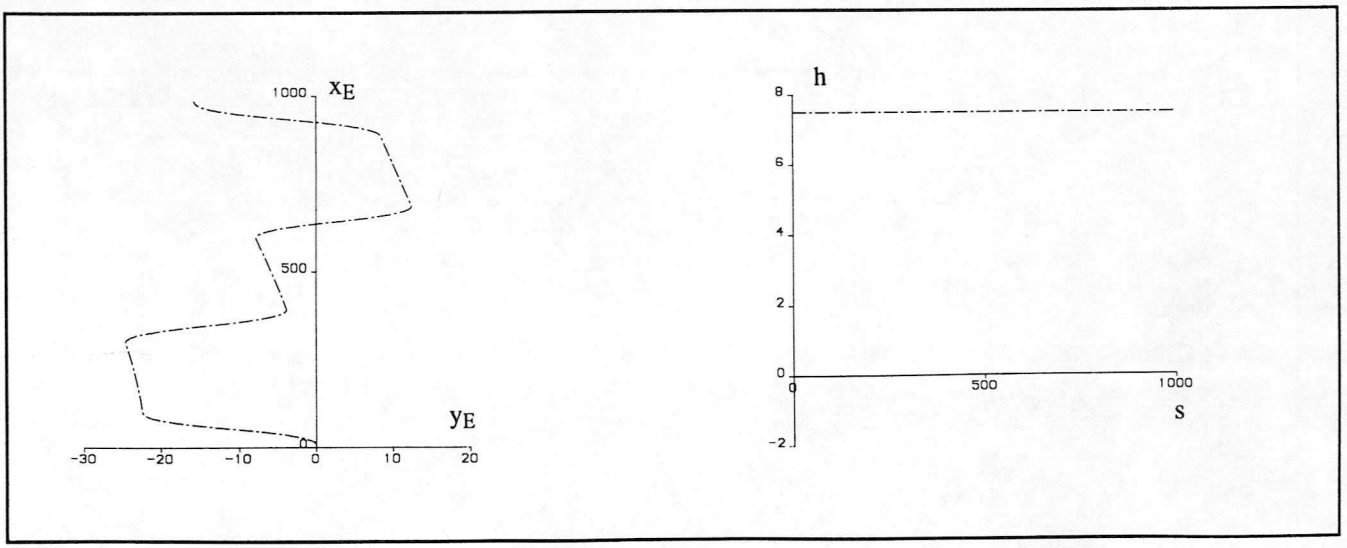

Figure 11 Track and Altitude Calculated by *Genisa* for Cases 1, 2 and 3
v_E vs. x_E and h vs. s (m)

Appendix A The Conceptual Simulation Model (CSM)

The CSM is documented more comprehensively within reference [2]. Readers unfamiliar with the model are advised to use [2] in tandem with this report.

A.1 Introduction

Conventional helicopters are characterised by marked non-linearities and cross-coupling in their dynamic response. The demanding environment of nap-of-the-earth (NOE) flying can impose a high workload on the pilot. Advanced control systems present the opportunity to reduce workload and more fully exploit the aircraft's performance. It is necessary however, to obtain a comprehensive understanding of which control modes would be most suited to NOE flight. The complexities of a non-linear model make prediction of control responses very difficult. It was deemed appropriate to develop a greatly simplified 'conceptual' model, so easing investigation of different control systems. The optimum controls thus identified can be adapted for more 'realistic' models in due course.

Cockpit ergonomics will not be discussed here as this inverse simulation is concerned only with the control inputs, helicopter state responses and flight path outputs i.e. the mathematical model summarised by equations (1) and (2).

The ability to precisely control the pitch, roll and yaw of the helicopter is a fundamental requirement for fast and accurate adherence to flight path. Within the CSM, the angular responses are represented by simple transfer functions which act on the longitudinal, lateral and pedal control inputs. In this way the type and mode of control can be easily varied and simply defined using parameters directly related to the vehicle response characteristics (e.g. frequency and damping). Cross coupling is completely absent; the idea being that the control system in a real ACT helicopter could completely suppress such effects.

It was considered too abstract to represent the rotor thrust by transfer functions acting on the collective input, especially as the basic rotor response to collective pitch can be modelled quite simply. Additionally the simple rotor model allows calculation of the power absorbed by the rotor. Thrust sensitivity is assumed to include the cyclic pitch needed in practice to balance the moments generated by collective.

Turn coordination and normal force augmentations were used to minimise the cyclic and collective inputs required to maintain speed and height, thus easing control

in turning flight. In essence then the helicopter is motivated by a thrust vector parallel to the rotor shaft, the magnitude of which is altered by the collective input, the direction by using the angular inputs.

A.2 Rotational Freedoms

The control laws used within the CSM depend upon the helicopter velocity. However, as the lateral jinking manoeuvre discussed in this report is flown at a constant 60 knots, only the relevant control law (rate demand) will be discussed.

i) Pitch

Within the CSM there is a deadspace function which describes an area of insensitivity about the control mid-stick positions. It should be noted that all controls calculated by *Genisa* are the effective values i.e. control values equal to zero could be anywhere within the deadspace.

The demanded pitch rate is the following function of the longitudinal control input, η and the gains, G which vary according to the helicopter to be represented.

$$q_{DEM} = G_q \eta + G_{q^3} \eta^3, \qquad \eta_{MAX} = \pm 1 \tag{A-1}$$

Simple first order actuator model gives finite pitch acceleration.

$$\dot{\eta}_{1s} = \frac{q_{DEM} - \eta_{1s}}{\tau_a} \tag{A-2}$$

Pitch acceleration .

$$\dot{q} = M_{TC} - M_q (\eta_{1s} + q_{DEM_{TC}} - q) \tag{A-3}$$

The turn coordination terms $q_{DEM_{TC}}$ and M_{TC} are defined in §A.4, the derivative M_q depends on the helicopter being modelled.

ii) Roll

The demanded roll rate is the following function of the lateral control input ξ.

$$p_{DEM} = G_p \xi + G_{p^3} \xi^3, \qquad \xi_{MAX} = \pm 1 \tag{A-4}$$

Simple first order actuator model gives finite pitch acceleration.

$$\dot{\eta}_{1c} = \frac{p_{DEM} - \eta_{1c}}{\tau_a} \tag{A-5}$$

Roll acceleration .

$$\dot{p} = - L_p (\eta_{1c} + p_{DEM_{TC}} - p) \tag{A-6}$$

The turn coordination term $p_{DEM_{TC}}$ is defined in §A.4, the derivative L_p depends on the helicopter being modelled.

iii) Yaw

The demanded yaw rate is the following function of the lateral control input ζ.

$$r_{DEM} = G_r \zeta + G_{r3} \zeta^3, \qquad \zeta_{MAX} = \pm 1 \tag{A-7}$$

Simple first order actuator model gives finite pitch acceleration.

$$\dot{\eta}_{0TR} = \frac{r_{DEM} - \eta_{0TR}}{\tau_a} \tag{A-8}$$

Roll acceleration .

$$\dot{r} = N_{TC} - N_r (\eta_{0TR} + 2.0 \dot{\beta} - N_r \beta) \tag{A-9}$$

The turn coordination term N_{TC} is defined in §A.4, the derivative N_r depends on the helicopter being modelled.

A.3 Translational Freedoms

i) Rotor Model

The rotor thrust is based upon conventional blade element / momentum theory [5], [6] though much simplified. Forces normal to the shaft, both longitudinal and lateral flapping and rotor in-plane forces, are neglected. Constant rotor speed is assumed. Asymmetric disc loadings are ignored as an effective control system would

suppress this feature. A simple inflow model is used but no fuselage downforce due to the downwash is considered. Rotor flow parameters are calculated from airspeed components resolved through rotor shaft tilt (small angle approximation assumed). Note that the range of δ_C is $0 \rightarrow +1$.

Velocity components.

$$u_{BR} = u_B + w_B\,\theta_{SHAFT} \tag{A-10}$$

$$w_{BR} = w_B - u_B\,\theta_{SHAFT} \tag{A-11}$$

Non-dimensionalised velocity in the plane of, and normal to the rotor disc.

$$\mu = \frac{\sqrt{u_{BR}^2 + v_B^2}}{\Omega R} \tag{A-12}$$

$$\mu_z = \frac{w_{BR}}{\Omega R} \tag{A-13}$$

Normalised induced inflow, and thrust coefficient used in Newton-Raphson iterative solution for λ_0.

$$\lambda_0 = \frac{C_{T\,inflow}}{2\sqrt{\mu_2 + (\mu_z - \lambda_0)^2}} \tag{A-14}$$

$$C_{T\,inflow} = \left[\delta_c\left(\frac{1}{3} + \frac{1}{2}\mu^2\right) + \frac{1}{2}\left(\mu_z - \lambda_0\right) + \frac{1}{4}\left(1 + \mu^2\right)\theta_{tw}\right]\frac{a_0\,s}{2} \tag{A-15}$$

Thrust coefficient used to calculate normal force. The term $\delta_{c_{TC}}$ is defined in §A.4.

$$C_T = \left[\left(\delta_c + \delta_{c_{TC}}\right)\left(\frac{1}{3} + \frac{1}{2}\mu^2\right) + \frac{1}{2}\left(\mu_z - \lambda_0\right) + \frac{1}{4}\left(1 + \mu^2\right)\theta_{tw}\right]\frac{a_0\,s}{2} \tag{A-16}$$

X force coefficient.

$$C_X = \left(-\delta_0 + \delta_2\,C_T^2\right)\frac{\mu s}{4} \tag{A-17}$$

The rotor X and Z forces are resolved into the reference body axes, again assuming small shaft tilt angle and neglecting the lifting component of rotor drag.

$$X_{ROT} = (C_X + C_T \theta_{SHAFT}) \pi \rho R^4 \Omega^2 \quad \text{(A-18)}$$

$$Y_{ROT} = 0 \quad \text{(A-19)}$$

$$Z_{ROT} = - C_T \pi \rho R^4 \Omega^2 \quad \text{(A-20)}$$

ii) Fuselage Model

Local incidence and airspeed are dependent on rotor induced velocity :

$$w_I = - \lambda_0 \Omega R \quad \text{(A-21)}$$

$$\alpha_F = \tan^{-1} \left(\frac{w_B + G_\lambda w_I}{u_B} \right) \quad \text{(A-22)}$$

$$V_F = \sqrt{u_B^2 + v_B^2 + (w_B + G_\lambda w_I)^2} \quad \text{(A-23)}$$

Fuselage forces.

$$X_{FUS} = \frac{1}{2} \rho V_F^2 S_{XF} C_{XF} \cos \alpha_F \quad \text{(A-24)}$$

$$Y_{FUS} = \frac{1}{2} \rho V_F v_B S_{YF} C_{YF} \quad \text{(A-25)}$$

$$Z_{FUS} = 0 \quad \text{(A-26)}$$

iii) Total Forces

$$X_{TOT} = X_{FUS} + X_{ROT} \quad \text{(A-27)}$$

$$Y_{TOT} = Y_{FUS} \quad \text{(A-28)}$$

$$Z_{TOT} = Z_{ROT} \quad \text{(A-29)}$$

A.4 Turn Coordination Terms

The turn coordination facility is intended to reduce workload by causing the vehicle to execute a true balanced turn in response to an input on a single inceptor. Required turn rate is defined as a function of the instantaneous bank angle, ϕ and suitable moments are produced to achieve appropriate pitch, roll and yaw rates for a correctly banked turn. Acceleration terms are included to ensure the correct transient dynamics. The choices of both rate and acceleration terms are described in [2].

i) Maximum Bank Angle.

During a coordinated turn the required pitch rate becomes infinite at 90° of bank. To avoid this singularity a maximum bank angle, ϕ_{TC} is set at 70°. Beyond ϕ_{TC} its tangent is used, angles above 90° are replaced by their complements.

ii) Steady State Angular Rates.

Pitch, roll and yaw rates appropriate to current bank angle.

$$p_{DEM_{TC}} = \frac{g \cos\gamma \tan\phi_{TC} \sin\theta}{V_T \cos\beta} \quad \text{(A-30)}$$

$$q_{DEM_{TC}} = \frac{g \cos\gamma \tan\phi_{TC} \sin\phi}{V_T \cos\beta} \quad \text{(A-31)}$$

$$r_{DEM_{TC}} = \frac{g \cos\gamma \sin\phi}{V_T \cos\beta} \quad \text{(A-32)}$$

ii) Angular Accelerations During Turning Manoeuvre.

$$M_{TC} = \frac{2\, g \sin\phi\, (p \cos\gamma + r \sin\gamma)}{V_T \cos\beta} \quad \text{(A-32)}$$

$$N_{TC} = \frac{g\,(p \cos\gamma \cos\phi + r \sin\gamma)}{V_T \cos\beta} - \left(\frac{g}{V_T \cos\beta}\right)^2 \left\{\cos\gamma \sin\phi \left[\frac{X_{TOT} \cos\alpha + Z_{TOT} \sin\alpha}{m\, g} - \sin\gamma + \frac{r\, v_B}{g}\right]\right\} \quad \text{(A-33)}$$

iii) Collective Augmentation.

The following augmentation term increases collective to ensure that, when the helicopter is banked, the vertical component of rotor thrust balances the weight. This term is not included in the inflow calculation, so that when activated a power increase is still registered.

$$\Delta Z_{ROT_{TC}} = m\ g \cos\theta\ (\tan\phi_{TC} \sin\phi + \cos\phi - 1) \tag{A-34}$$

$$\delta_{c_{TC}} = \frac{\Delta Z_{ROT_{TC}}}{\left(\frac{1}{3} + \frac{1}{2}\mu^2\right)\left(\pi \rho R^4 \Omega^2 \frac{a_0 s}{2}\right)} \tag{A-35}$$

Appendix B Configurational and Control Data

Parameter and Symbol		Values	Units
Rotor lift-curve slope	a_0	6.0	(1/rad)
Fuselage X-force coefficient	C_{XF}	- 0.16	
Fuselage Y-force coefficient	C_{YF}	- 0.75	
Fuselage to rotor downwash	G_λ	1.5	
Mass	m	4078.86	(kg)
Rotor radius	R	6.4	(m)
Rotor solidity	s	0.0778	
Fuselage plan area	S_{XF}	13.84	(m2)
Fuselage side area	S_{YF}	19.14	(m2)
Rotor drag factor	δ_0	0.009	
Rotor induced drag factor	δ_2	5.333	
Rotor shaft tilt angle	θ_{SHAFT}	0.0698	(rad)
Rotor speed	Ω	35.63	(rad/s)

Table 1 Fuselage and Rotor Parameters

Parameter and Symbol		Values	Units
Roll			
Roll rate demand linear gain	G_p	1.0	(rad/s)
Roll rate demand cubic gain	G_{p^3}	1.0	(rad/s)
Roll derivative	L_p	- 4.5	(1/s)
Pitch			
Pitch rate demand linear gain	G_q	1.0	(rad/s)
Pitch rate demand cubic gain	G_{q^3}	1.0	(rad/s)
Pitch derivative	M_q	- 9.0	(1/s)
Yaw			
Yaw rate demand linear gain	G_r	1.0	(rad/s)
Yaw rate demand cubic gain	G_{r^3}	1.0	(rad/s)
Yaw derivative	N_r	- 4.5	(1/s)

Table 2 Control Laws

References

1. Rutherford, S., Thomson, D.G., "Development of a Generic Inverse Simulation Algorithm.", Internal Report No. 9410, July 1994.

2. Buckingham, S.L., Padfield, G.D., "Piloted Simulations to Explore Helicopter Advanced Control Systems.", Royal Aerospace Establishment, TR 86022, April 1986.

3. Cheney, W., Kincaid, D., "Numerical Mathematics and Computing. Second Edition.", Brooks/Cole Publishing, 1985.

4. Press, W. H., Teukolsky, S. A., Vetterling, W. T., Flannery, B. P., "Numerical Recipes in Fortran. The Art of Scientific Computing. Second Edition.", Cambridge University Press, 1986.

5. Padfield, G.D., "A Theoretical Model of Helicopter Flight Mechanics for Application to Piloted Simulation.", Royal Aerospace Establishment, TR 81048, April 1981.

6. Thomson, D.G., "Development of a Generic Helicopter Model for Application to Inverse Simulation", Internal Report No. 9216, June 1992.